

T. RAMKUMAR^{1*}, S. MADHUSUDHANAN¹, I. RAJENDRAN¹

EFFECT OF NICKEL ON THE MICROSTRUCTURE, MECHANICAL AND TRIBOLOGICAL PROPERTIES OF AUSTEMPERED DUCTILE CAST IRON FOR STEERING KNUCKLE APPLICATIONS

The research article address, the mechanical properties such as fatigue, impact strength and tribological properties of Austempered ductile iron (ADI) has been investigated. The samples of ADI iron were austenitized at 927°C for 2 hrs and later it was under austempering process for 2 hrs at a temperature range of 240°C to 400°C. Experiments under axial loading has been carried out on three different compositions (without Ni(X), 0.22 wt % Ni (X₁), 0.34 wt. % Ni (X₂). Fabricated test bars were converted in to as per ASTM standard samples for different tests. In order to study the influence of chunky nickel morphology studies on fatigue life and impact strength were carried out on a second set of specimens without any microstructural defect. Metallurgical analyses were performed on all the samples of heat treated samples (AF – Ausferrite, MB – Mixed bainite, M – Martensite, RA – Retained Austenite and N-Nodule) were found and compared. It was found that a mean content of 22% of chunky nickel in the microstructure (with respect to total Ni content) influence considerably the fatigue and impact strength properties of the cast iron. Moreover tribological properties of the specimens were also studied under dry sliding conditions at various sliding speed and load. The wear resistance and coefficient of friction were found to increase with increase in load and sliding speed.

Keywords: Austempered ductile iron, Fatigue, Impact, Ni, surface transition, wear

1. Introduction

Among industrial alloys, cast iron has the most diverse mechanical properties with the cheapest price. The need of industry to achieve structures with higher strength and flexibility led to the beginning of extensive research to change the structure of these ductile irons. Austempering is a process of heat treatment that creates bainite structure in iron and the purpose of this operation is to improve the mechanical properties such as strength, impact resistance, flexibility and wear resistance.

The results revealed that alloy has a combination of desirable mechanical properties as well as good wear behavior. In fact, austenite microstructure (ferrite blades in austenite field) along with the amount of residual austenite is considered as the main factor of increasing the strength and high wear resistance of this alloy [1]. Wear rate decreases with increase the austempering time for a given austempering temperature which increases with increase in austempering temperature [2]. Modern materials used to create the elements of machinery, equipment and vehicles (cars, trucks, tractors, etc.) must possess, in addition to high hardness, a good toughness and a high fatigue strength, as well as

amore satisfactory resistance to friction and wear [3,4]. The wear resistance of the ductile cast iron can be enhanced by different heat-treatment procedures and surface engineering techniques, each with some limitations and drawbacks [5]. Austempering in steel lead to upper or lower bainite microstructures which include needle ferrite together with tiny carbide participates [6]. Wear rate is dependent on the yield strength, austenite content and its carbon content [7]. The wear increased with decreasing the austempering time [8]. Isothermal quenching at high temperatures, i.e. at 370°C and 320°C, makes the ductile iron more resistant to abrasion in the dry corundum environment when nickel and molybdenum are added. Low temperature of isothermal quenching, at 270°C permits obtaining the highest level of abrasion wear resistance in the ductile iron with copper and nickel [9]. ADIs have very high dry sliding wear resistance which equals with the resistance of very hard steels.

The aim of the performed investigation is to study the influence of alloying elements on the microstructure, wear, and mechanical properties of the produced austempered ductile cast iron. The relationships among the alloying elements, Nodularity, Pearlite% and mechanical properties were correlated. The

¹ DEPARTMENT OF MECHANICAL ENGINEERING, DR. MAHALINGAM COLLEGE OF ENGINEERING AND TECHNOLOGY, POLLACHI, TAMILNADU 642 003, INDIA

* Corresponding author: ramkimech@gmail.com



disc was manufactured based on % of Ni and two types of pins (31HRC & 62 HRC) hardness pins were used for the test. Wear rate and coefficient of friction were compared with different velocity and speed.

2. Materials and methods

2.1. Materials

Ductile iron disc samples of three different composition (X – without Ni, X₁ – Ni-0.22%, X₂ – Ni 0.34%) were produced from commercial foundry and were used this experiment. The chemical composition of ASTM specimen is given in Table 1.

2.2. Fabrication process

The ASTM bars and wear discs were developed through casting process. The spheroidal graphite iron (SG) liquid metal temperature was raised up to 1530°C and nickel of 0.22% wt and 0.34% wt were added in to the furnace. The temperature was raised to 1540°C and the molten metal taped into moulds. The Fig. 1 shows the tapping process of the metal. After that components were removed from the moulds as the temperature dropped below 800°C and allowed for natural cooling. The discs were removed from the moulds and sent for de-heading process. Later, the separated components moved to shot blasting for cleaning purpose. The composition was found out by spectrometer analysis. Then wear discs were also heat treated and converted in to ADI.

The machining of wear discs is very difficult after ADI heat treatment process compared to as cast condition. Hence special types of milling tool were used for the machining purpose. The wear test samples were prepared according to ASTM G-99 standard. Final surface finish was obtained by surface grinding process.

2.3. Austempering process

Austempering is a heat treat process that improves the properties of ductile iron. Austempering, requires:

- Minimum nodule count (100 /mm²) which minimizes segregation of alloy elements that can increase the presence of carbides and delay the rate of formation of the Ausferrite microstructure
- Minimum nodularity (85%) which will inhibit the formation of porosity or micro shrinkage and support the formation of small and round graphite nodules.
- Consistent chemistry which is required for repeatability. The chemistry of the iron plays an important role in establishing the as-cast microstructure of the component. The relative amounts of ferrite and pearlite in the as-cast material affected the growth of the component with austempering.

The samples of ADI iron were austenitized at 927°C for 2 hrs. and then it was under austempering process for 2 hrs. Then it was suddenly transferred to a salt bath at a range of 240°C to 400°C. The samples were then cooled in air to reach the room temperature. Then the samples were cleaned from residual salt by dipping them in a water bath at room temperature.

TABLE 1

Chemical composition of material used for the study

Discs	C	Si	Mn	S	Cr	Ni	Cu	Mg	Zn	Ag	Co	Fe
X (%)	3.63	2.63	0.22	0.008	0.029	0.013	0.09	0.046	0.062	0.004	0.004	93.13
X ₁ (%)	3.64	2.57	0.39	0.007	0.029	0.228	0.75	0.042	0.042	0.005	0.004	92.21
X ₂ (%)	3.58	2.61	0.35	0.008	0.032	0.341	0.7	0.046	0.03	0.005	0.004	92.29



Fig. 1. Fabrication process

2.4. Microstructure

Metallographic samples were cut from heat treated samples. Initially Specimens were polished using belt polisher and later by emery papers of various grid sizes such as 600, 800 and 1200 respectively. Finally velvet cloth polishing was used with alumina slurry and diamond paste. Metallographic images were made using computer integrated Olympus optical microscope (100×) and the distributions of particles were observed by JEOL 6390 scanning electron microscope. The worn surfaces of each specimen under various loading conditions were studied using optical microscope at 200×.

2.5. Mechanical Studies

The tensile specimens were prepared and test was conducted based on ASTM standard of E-08 [11]. Tensile test was conducted for 7 identical samples with circular cross section with 5 mm dia. and 25 mm gauge length. After machining, the specimens were polished using emery papers to generate fine surface finish without any scratches. The tests were carried out at a constant rate ($4 \times 10^{-4} \text{ s}^{-1}$) using (MTS) servo-hydraulic machine in ambient atmosphere. Load-displacement plots and yield strength, ultimate tensile strength and percent-elongation values were calculated from these load-displacement diagrams. The average values from seven test samples are reported.

Fatigue test was carried out for three compositions (X , X_1 & X_2) of steering knuckles using suitable test rig. High cycle fatigue tests were conducted on steering knuckle at $\pm 4.7 \text{ KN}$ up to 1×10^7 cycles and no damage was recorded. The test results met the industrial standard [12].

The impact test was performed using dynatup with suitable fixtures. A drop weight of 87.5 kg and a velocity of 5.03, 5.34, 5.63 m/s were chosen. The impact time was of very short duration in the range of milliseconds and data acquisition card was used to record the impact load, energy absorbed and deflection of the component.

2.6. Wear test

A pin on disc wear testing machine was used to study the dry sliding wear behavior of different ADI samples which was made by Ducom industries and is shown in Fig 2. Wear tests were carried out as per ASTM G99 standards. Contact surfaces

were prepared by grinding them against silicon carbide paper and acetone were used to clean the disc and maintained constant contact area between the pin and the disk during wear and provides: (i) removal of wear debris, (ii) uniformity of surface conditions (iii) easy wear measurement and (iv) easy specimen fabrication. The specimen of mild steel pin and HSS pin with a hardness of 31HRC and 62 HRC with 8 mm dia. and 15 mm height of pin were used for testing. Three type of discs (Fig. 2) of 12 mm thickness and 100 mm dia. were used as counterpart of hardness of 326, 380, 358 VHN. During the test, the pin was pressed against the disc with variable load of 50 N, 60N and 80 N. The sliding speed of the discs was selected as 1.57 m/s, 2.67 m/s and 3.76 m/s. A track dia. of 60 mm and distance of 1800 m were selected for this test. The specimen was tightened and care has been taken so that cross section of the specimen was in contact with the disc during the experiment. The weight loss method was used to find the wear rate in gm/min. At the end of each test, the disc was cleaned and its final mass was determined. The difference between the initial and final mass of the disc gave the mass loss due to sliding wear. The weight loss experienced by the ADI under each composition was observed. Wear rate and coefficient of friction was calculated for various speed conditions. All experiments were carried out under atmospheric temperature. Two different hardness pins were used to evaluate the tribological behaviour of ADI and as shown in Table 2.

TABLE 2

Chemical composition of Pins used for the study

Composition Pin Material	C	Mn	Si	V	Mo	Fe
HSS Steel	2-2.5	0.25-0.3	0.25-0.3	0.2	0.8	Bal.
Mild Steel	0-0.25	0.4-0.7	0.1-0.5			Bal.



Fig. 2. Wear testing machine and Wear discs of three compositions

Wear surface morphology was taken through optical Electron Microscope. Then difference between non-deformed and deformed samples of ADI under each composition was analyzed.

Wear rate and co-efficient of friction were determined using the Eq. (1) & (2):

$$\text{Wear rate} = \text{Weight loss} / \text{Sliding distance (g/m)} \quad (1)$$

$$\text{Coefficient of friction} = \text{Frictional force} / \text{Applied load} \quad (2)$$

2.7. Wear morphology and its mechanisms

Wear is the process of removal of solid metal from one or both surfaces which are in solid state contact and is defined as mild and severe wear. In mild wear the worn surfaces are smooth and wear debris is small (typically 0.01-1 μm in particle size) while in contrast, the severe the wear larger is the wear debris size (20-200 μm). The important wear mechanisms are abrasive, oxidative, adhesive and delamination wear. It occurs due to hard particles or protuberances sliding along a soft solid surface that results from ploughing, wedging and cutting phenomena. In tribological systems, grooves on one or both of the contact surfaces as the debris is entrapped between the contact surfaces. In oxidative environment oxidative wear occurs when sliding

takes place due to the oxygen present in the normal environment or other which may react with the solid surface. Fatigue/Delamination wear is caused by fracture arising from surface fatigue under cyclic loading which results in a series of pits or voids. A crack on the subsurface or the surface is caused due to repeated cyclic loading. The subsurface cracks proliferate and connect with other cracks to reach the surface to generate wear particles. Surface cracks can travel downward into bulk and connect with other cracks to form a wear particle. When a hard rough surface slides over a soft metal surface frictional resistance is mainly developed. The friction coefficient is the force necessary for the plastic flow of the softer material. The ploughing of the surfaces by hard asperities and wear particles are the most important mechanism in most sliding situations.

3. Results and discussion

3.1. Microstructure examination

The microstructures of heat treated specimen were observed as shown in Fig. 3(a-c), which reports the microstructure of heat treated samples. Fig. 4(a), (b) & (c) shows the SEM analysis results which confirm the matrix seen in the microstructure.

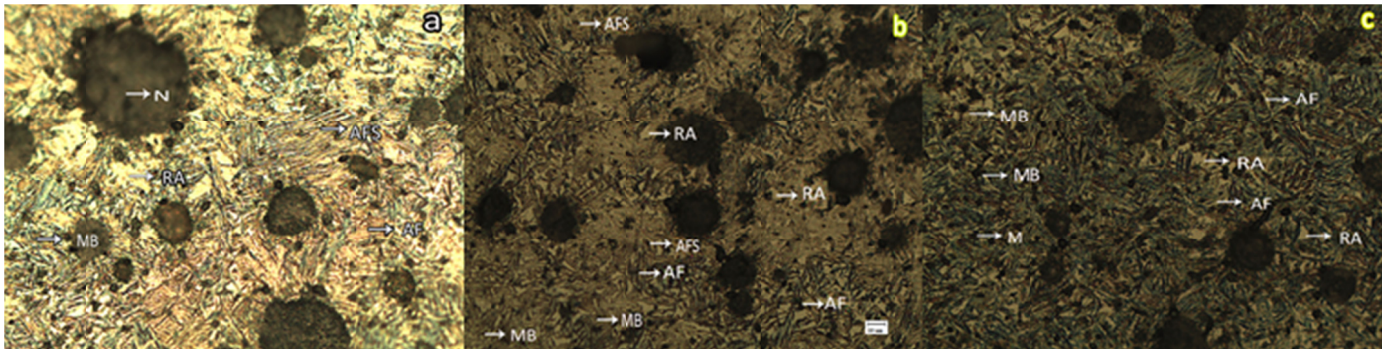


Fig. 3. Heat treated sample microstructure (AF – Ausferrite, MB – Mixed bainite, RA – Retained Austenite, N – Nodule)

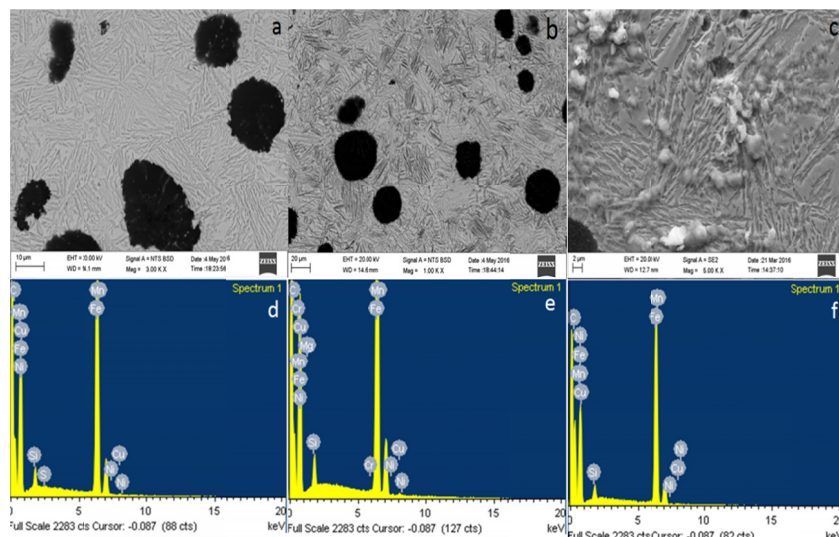


Fig. 4. SEM Analysis of samples (a) X (b) X₁ (c) X₂ and EDAX analysis of samples (d) X (e) X₁ (f) X₂

TABLE 3

Mechanical properties, Hardness of heat treated and microstructure analysis of the before heat treatment samples

Specimen	UTS (Mpa)	YTS (Mpa)	Elongation (mm)	E ($\times 10^5$) (N/mm ²)	Hardness (VHN)	Ferrite (%)	Pearlite (%)
X	479	318.9	14.9	1.78429	326	60-65	35
X ₁	870	558.7	8.02	1.91402	380	15-20	85-90
X ₂	855	525.25	7.25	1.81893	358	20	75

Fig. 4(d), (e) & (f) shows the EDAX analysis that reports the availability of Ni and Cu in the composition.

As per the analysis, all the three irons X, X₁, X₂ have adequate carbon content (3.64%) and nodularity was observed up to 90-95%. The volume fraction of graphite was $10 \pm 0.8\%$ with an average diameter of $23.5 \pm 5 \mu\text{m}$. Due to higher carbon content compared to general composition, all the three irons showed nodule counts from 125 to 150 Nos/mm² and the average size of 3 to 4 as per ASTM. Before heat treatment, metallographic analysis shows that all the three irons were mixture of pearlite and ferrite. Table 3 shows the % of ferrite and pearlite mixture in the before heat treated specimen.

After isothermal process of X₁ (0.22% Ni) sample at 380°C lower bainite and retained austenite were noticed. In Sample X₂ (0.34% Ni) upper bainite and retained austenite were observed. The content of retained austenite decreased slightly which may be due to the % of nickel which influences grain refinement. But no change in nodule shape, count and size was observed [22].

The change in mechanical properties after isothermal heat treatment caused changes in microstructure of specimens. Table 3 summarizes the mechanical properties of the austempered samples. This metal matrix showed decrease in the tensile properties and increase in hardness. Sample X₂ (0.34% Ni) showed lower bainite and retained austenite. Due to decrease in austenite %, the mechanical properties slightly decreased compared to X₁ and hardness increases. Similar results have been reported based on upper and lower bainite and retained austenite [12]. Compared with X, presence of alloying elements Cu and Ni stabilizes the formation of upper and lower bainite with retained austenite. The superior mechanical properties depend upon metal matrix of alloyed SG iron. Cu addition refines the grain structure and increases the mechanical properties.

3.2. Hardness

The micro hardness of the ADI with different composition is shown in table 3. The micro hardness values of ductile-iron depended on matrix constituents. Good wear resistance is obtained by high hardness. Low austempering temperatures (235-250°C) can produce hard ADI (~480-550 BHN) and such grades are selected where good wear resistance is the main requirement. The softer grades of ADI (typically 280-320 BHN) contain large amounts of austenite and harden and/or transform to martensite when subjected to mechanical strain at the surface, with increased wear resistance. The hardness variation based on Ni % is shown in Fig. 5 which shows that there is an appreciable increase in the

hardness of the matrix after austempering. Less hardness was observed for X (conventional DI) containing ferritic- pearlitic matrix (Fig. 3(a)) which may be due to varying proportions of pearlite and ferrite, and increase in the amount of pearlite in the iron increased the macro hardness [21].

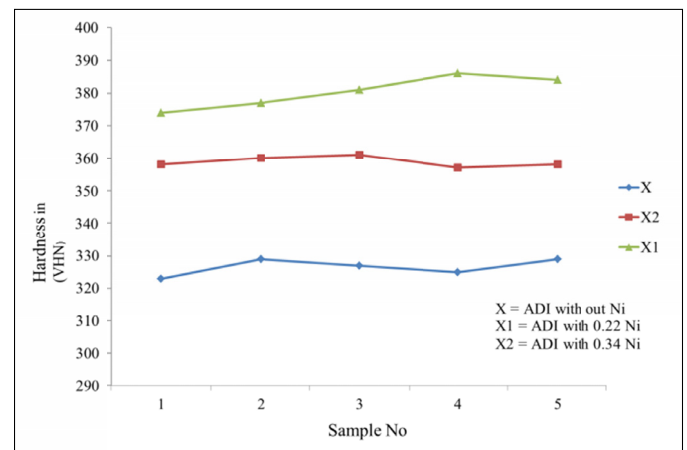


Fig. 5. Hardness variation of ADI sample

The austempered samples hardness with lower bainitic structure was higher than the samples with upper bainitic structure. The hardness of the austempered samples, with upper bainitic structure changed from 358 to 361 HV(X₂) and that of the samples with lower bainitic structure changed from 374 to 386 HV(X₁). With increase in Ni %, hardness of ADI increased [20]. It is found that the abrasion wear resistance increases (weight loss decreases) as hardness increases [23].

3.3. Tensile test

The significant improvements in the properties of ductile iron brought about by austempering are apparent. For example, when austempered at 375°C, the hardness and tensile strength are nearly doubled although the toughness and elongation decreases marginally. In the tensile test, three samples X, X₁, X₂ in each composition 7 specimens were prepared and tested based on ASTM standard E-466 and is shown in Fig. 6(a). The study shows that the nickel addition plays a very important role on tensile properties.

Based on the test (Refer Fig. 6(b)), UTS values of X₁ increased to 81% and YTS increased to 75% but elongation decreased from the base iron X. which may be to lower bainite and retained austenite. UTS value of X₂ increased to 78% and

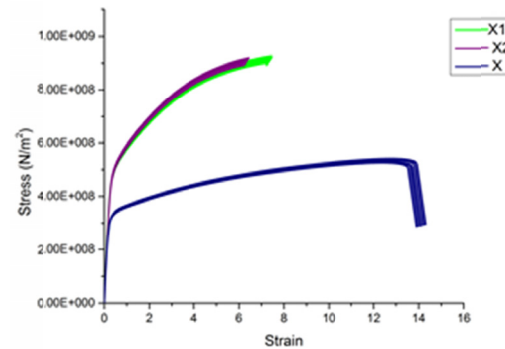


Fig. 6. a) Tensile test specimen as per ASTM standard and b) Stress Vs Strain curve for ADI

YTS increased to 65% from the base X but elongation decreases compared to X and X_1 due to change of microstructure to upper bainite and retained austenite. Tensile strength was found to decrease with increasing austempering temperature for 120 mins. in all the grades. [19]. The stress and strain were high and elongation was less in X_1 compared to X. In X_2 Stress, Strain and elongation were less compared to X_1 . Ni addition increases the hardness and decreases the mechanical properties.

3.4. Fatigue test

The changes in microstructure of specimens after isothermal heat treatment cause a change in the mechanical properties. After isothermal processing of sample X_1 (0.25 % Ni) at 380°C, lower bainite and retained austenite were observed which increased the tensile properties and hardness. Sample X_2 (0.35% Ni) showed upper bainite and retained austenite. With decrease in austenite %, the mechanical and hardness properties slightly decreased compared to X_1 . Compared with X, presence of alloying elements Cu and Ni stabilizes the formation of upper and lower bainite with retained austenite in X_1 and X_2 . The superior mechanical properties depend upon metal matrix of alloyed SG iron. Cu addition refines the grain structure and increases the mechanical properties. In fatigue process austenite plays an important role on ADI which allows extensive accumulation of plastic deformation and high fatigue resistance. Fig. 7 shows the various stress levels and life of the specimen. There is no fatigue limit at high cycle as fatigue stress amplitude decreases. Similar high cycle fatigues were conducted in three composition of steering knuckle at ± 4.7 KN up to 1×10^7 cycles and no damage was observed. The stabilization of retained austenite, bainites and martensites around the graphite nodules has been supported by grain refinement of alloyed SG iron which helps in improvement of fatigue strength of the steering knuckle. The fatigue results were already published elsewhere in my previous work.

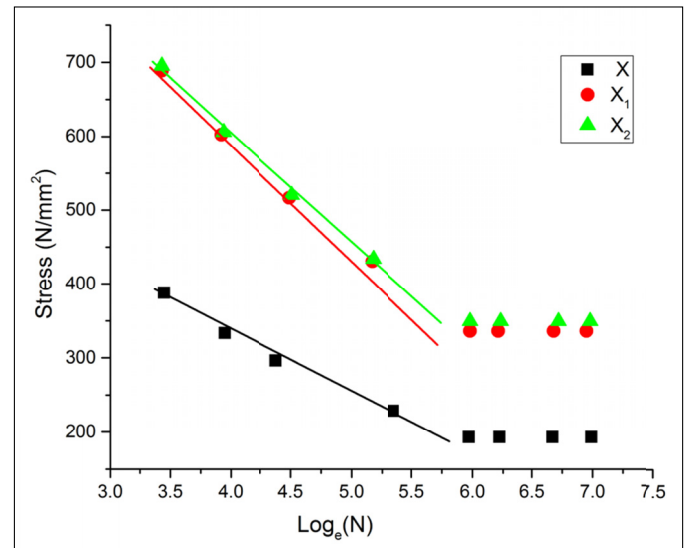


Fig. 7. S-N curves of ADI samples

3.5. Impact Test

The steering knuckle impact test was carried out on three different compositions of ADI namely (X, X_1 & X_2) knuckles. For each velocity and impact energy 5 samples were tested. The impact test results are summarized in Table 4. Fig. 8 shows the test results as energy versus deflection graphs at an impact velocity of 5 m/s, 5.34 m/s, 5.63 m/s & 5.94 m/s. The deflection increased with increase in the impact energy of the test. The deflection of X knuckle is comparatively higher than X_1 , and X_2 . At 5 m/s velocity and 800 J impact energy condition deflection varied as X – 5 mm, X_1 – 4.5 mm, X_2 – 4.1 mm. In this test deflection of X_1 was lower compared to X and X_2 . At 5.34 m/s velocity and 900 J impact energy condition deflection varied as X – 7.5 mm, X_1 – 5.8 mm, X_2 – 5.3 mm. At 5.63 m/s velocity and 1000 J impact energy condition deflection varied as X – 9 mm, X_1 – 7 mm, X_2 – 6 mm, an 5.94 m/s velocity and

1100 J impact energy condition deflection varied as X – 12 mm, X₁ – 9 mm, X₂ – 7.5 mm. For all four different velocities and impact energy test X₁ showed lower deflection compared to X and X₂. Which reports that Cu and Ni play a very important role in the impact test. Sample X has more deflection than X₁ and X₂ due to different microstructure compared to X₁ and X₂. The impact strength of steering knuckle increased with increasing the weight percentage of Ni in the steering knuckle.

TABLE 4

Summary of impact test results

S. No	Specimen	Velocity (m/s)	Energy (J)	Observation	Deflection (mm)
1	X	5	800	No Crack	5
2	X ₁			No Crack	4.5
3	X ₂			No Crack	4.1
4	X	5.34	900	No Crack	7.5
5	X ₁			No Crack	5.8
6	X ₂			No Crack	5.3
7	X	5.63	1000	No Crack	9
8	X ₁			No Crack	7
9	X ₂			No Crack	6
10	X	5.94	1100	No Crack	12
11	X ₁			No Crack	9
12	X ₂			No Crack	7.5

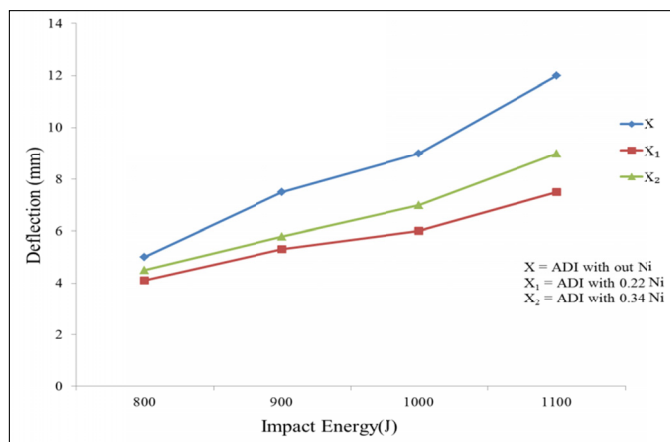


Fig. 8. Variation of deflection with respect to impact energy

3.4. Wear studies

3.4.1. Wear Rate

In the wear studies, wear rate was studied in the three composition of discs based on two different hardness pins. Fig. 9(a-c) shows the wear rate for hardness pin 62 HRC (d-f) shows the hardness for pin 31 HRC which shows wear rate as a function of sliding velocity at applied load of 50, 60, 70 N and 60 mm of track radius and sliding velocity of 1.57 m/s, 2.67 m/s, 3.76 m/s. All austempered specimens showed increase in wear rate as speed (velocity) increased [17]. The increase in speed changes heat generation that may affect the surface tem-

perature and surface properties of the specimen. Higher surface temperatures could increase the rate of oxidation and therefore change the wear mechanism to a milder wear when the speed of sliding increases. The wear factor was found to be higher for specimens which were tested at the higher load. The austenite to martensite transformation increases the strength at the surface rendering it able to withstand the high contact load, martensite is known to be brittle and is susceptible to cracking [18]. The ADI structure consists of upper bainite (X₂) and lower bainite (X₁) after austempering at 380°C for 2 hrs. The bainite is an oriented needle like grain structure of α -phase (bainitic ferrite), carbides and untransformed austenite [13]. The samples with upper bainitic structure showed hardness to range from 358 to 361 HV and lower bainitic structure hardness varied from 374 to 386 HV. The wear rate range for 50 N of pin 62, X varied from 1.26 to 1.95 $\times 10^{-5}$ mm³/m and pin 31 varied from 3.95 to 7.82 $\times 10^{-5}$ mm³/m, wear rate range for 70 N of X₁ (Pin62) varied from 1.34 to 2.42 $\times 10^{-5}$ mm³/m and pin 32 varied from 5.13 to 8.61 $\times 10^{-5}$ mm³/m, wear rate range for 80 N of X₂ (Pin62) varied from 1.42 to 2.6 $\times 10^{-5}$ mm³/m and pin 31 varied from 5.92 to 9.92 mm³/m. The wear rate of pin 31 is higher than pin 62 due to more weight loss in pin 62 than pin31. The disc hardness range varied from 326 to 380 VHN. The main factors that influence the wear rate are velocity, hardness, temperature and environmental conditions. The temperature plays a very important role in the wear rate because the velocity and load increases, temperature also increases. The wear rate increased with increasing the sliding speed and load of the test [16]. The wear rate increases in each specimen with load and speed increases but wear rate decreases with changing the composition of the material (X to X₂). The intensive strengthening decreased during the wear process due to dynamic strain, ageing of martensite and partial transformation of the metastable retained austenite in a strain-induced martensite [15].

3.4.2. Co efficient of friction (COF)

Fig. 10(a-c) shows the hardness pin 62 HRC (d-f) for hardness pin 31 HRC for COF as a function of sliding velocity at applied load of 50, 60, 70 N, 60 mm of track radius and sliding velocity of 1.57 m/s, 2.67 m/s, 3.76 m/s, COF increases with increase in sliding velocity and load. During sliding, the contact surfaces heat by friction and due the linkage of flat regions of the sliding surfaces, ploughing by wear particles and hard asperities occur. The frictional heating is continuous while the counter surface is in relative motion due to insufficient time for heat dissipation. As the flow ability of the material increases the sliding action is more and reduces the frictional heating and hence reduces the coefficient of friction.

COF value of 50 N load for specimen X, pin 62 varied from 0.65 to 0.75 and Pin31COF varied from 0.66 to 0.74. For specimen X₁, 70 KN load, pin 62 COF varied from 0.66 to 0.83 and pin 31 varied from 0.67 to 0.75. For specimen X₂, 80 KN load pin62 varied from 0.68 to 0.85 and pin 62 varied from 0.66

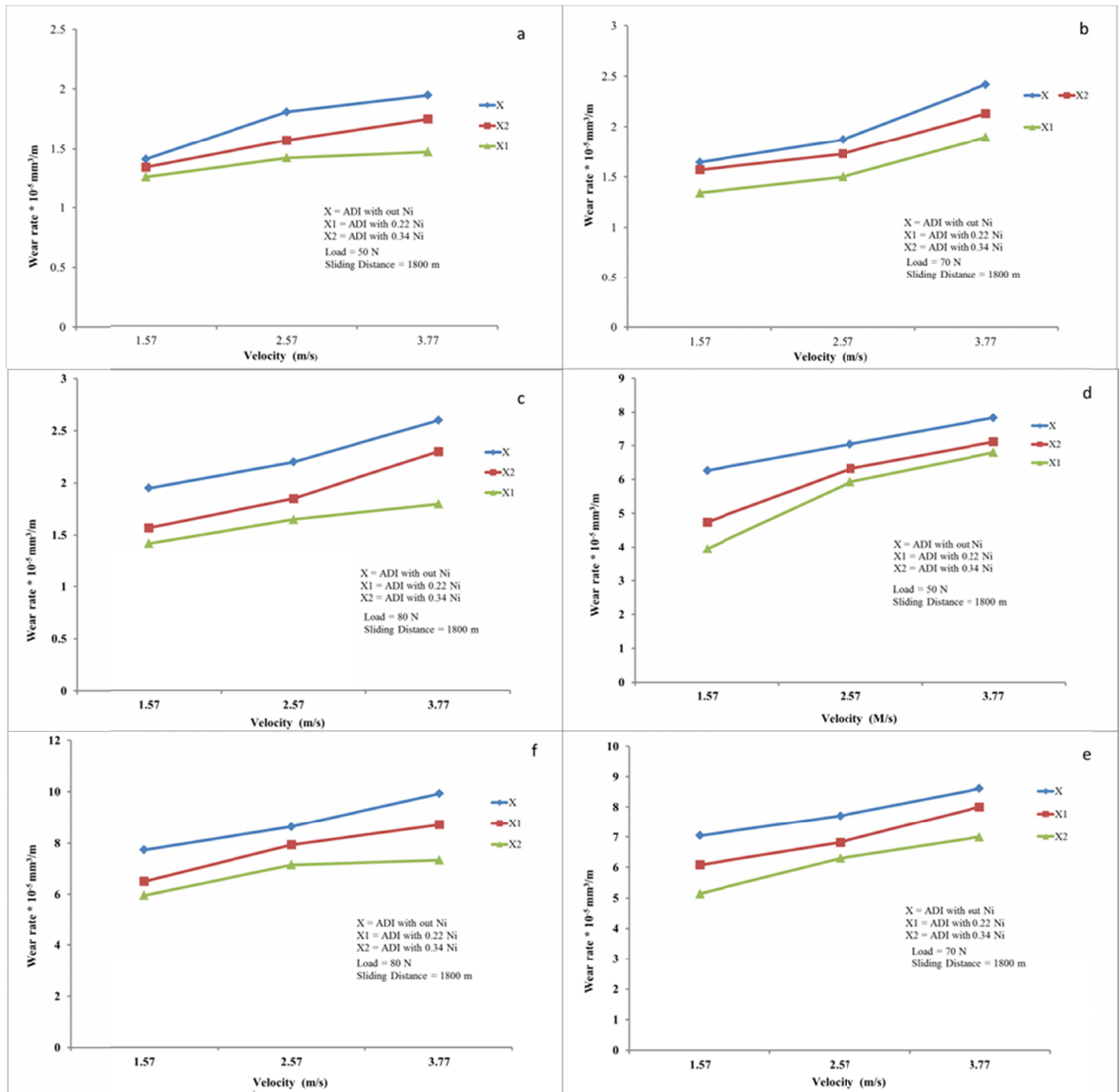


Fig. 9. Wear rate of ADI as a function of sliding speed for various loads, Pin 62 HRC (a, b, c), Pin 31 (d, e, f)

to 0.75. The velocity and load increase as mass loss was more and hence the COF increases slightly in each composition but decreases from X to X₂ because of mass loss decreases Ni % increases. The friction coefficient increased by increasing austempering temperature, thus the physical phenomenon of wear for low austempering temperatures was adhesive and abrasive wear and for high austempering temperatures was adhesive wear through formation of an intermediate or mixed layer. The temperature increased from ambient level, the coefficient of friction also increased irrespective of compositions because the coefficient of friction is mainly dependent on the pin temperature [24]. Moreover, the effect of surface fatigue on sliding condition helps adhesive and abrasive wear.

3.5. Wear morphology

The optical micrographs of the worn surface of ADI and the ADI-(0.22 % Ni and 0.34 % Ni) of the dry sliding wear are shown in Fig. 11 (a-c). Figure 11(a) shows that severe adhesive wear that takes place for the ADI as the material is ploughed out with an increasing load. In addition, the material has direct contact to the counterpart (HSS 62 HRC). During sliding over the hard counterpart, rigid particles are cracked and scattered in the sliding direction. It reveals the dominant plastic deformation of ADI without adding Ni content. Further, other two alloys such as (0.22% Ni and 0.34% Ni) show micro pits along the sliding direction, which significantly reduces the plastic deformation.

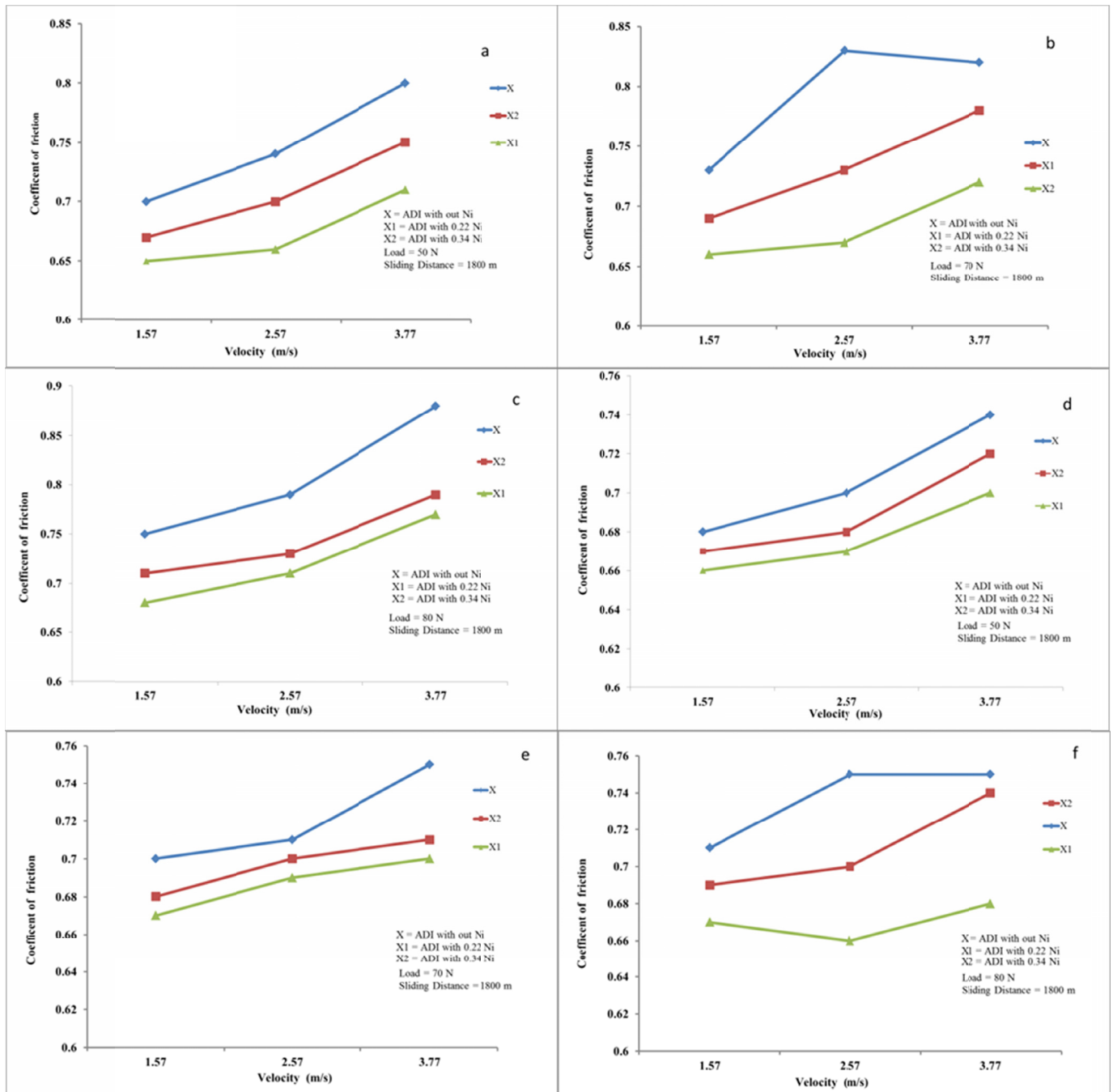


Fig. 10. Coefficient of friction as a function of sliding speed for various loads. Pin 62 HRC (a, b, c), Pin 31 HRC (d, e, f)

Fig. 11(b) shows the worn surface of 0.22% of Ni. It is very different from the normal ADI. There is no adhesion detected because the hardness of the alloy has been dramatically increased by adding Ni. The presence of tribo mechanically mixed layer converts the wear manner into a two body to three body wear and decreases the wear rate and reduces the coefficient of friction. This resulted in decrease of metal removal during wear test. It is perceived that the worn debris is more at without adding Ni which leads to increase the wear rate. In other words the occurrence of hard pulled out Ni particles formed on the steel disc acts as obstacle and further it converts the adhesive wear mode into abrasive mode. It is also perceived that less cracks

and scratches are present at the optimum condition (0.22% of Ni added ADI) of wear rate.

4. Conclusion

The following conclusion was drawn from study on micro structural aspects and wear behaviour of ADI due to the effect of austempering.

- Microstructural examination reveals the homogeneous distribution of Ni in the austempered ductile iron. EDAX analysis also confirms the Ni presence in ADI.

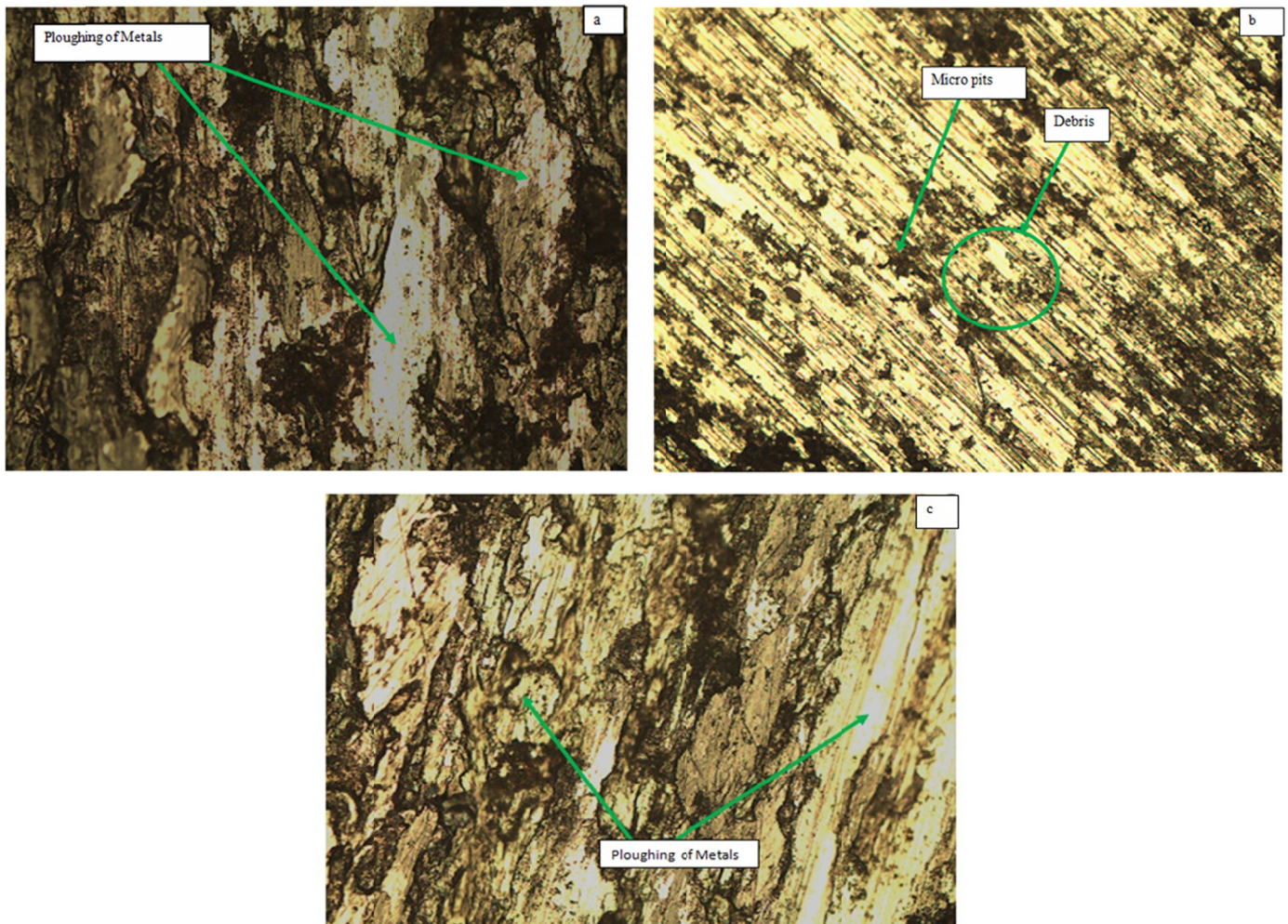


Fig. 11. OM micrographs of ADI a) without Ni, b) 0.22 % Ni and c) 0.34 % Ni of Pin 31 HRC

- While increasing the Ni in ADI the microhardness increased linearly. Microhardness of 0.22% of Ni added ADI possess significantly increasing hardness as compared to without Ni ADI and 0.34% Ni added ADI.
- Tensile strength measurements illustrated enhancement of mechanical properties due to the addition of Ni in ADI.
- S-N curve showed the fatigue strength of ADI. Fatigue strength of the sample X_1 was found to be high (326 MPa) compared to X and X_2 due to lower bainite and ausferrite structure.
- The three samples (X , X_1 , X_2) were compared using impact results which show, of the three samples, X_1 sample was found to absorb more energy for fracture compared to X and X_2 .
- The wear resistance depended on matrix structure and its hardness. The large ausferrite volume fraction with higher hardness resulted in lower wear rate.
- The abrasive weight loss increased approximately linearly with applied loads for as cast and ADI samples. The highest weight loss was observed for as cast sample due to a ferritic matrix with lowest hardness.

Acknowledgment

The authors thank the Management of Dr. Mahalingam College of Engineering and Technology, Pollachi, India for funding and M/s Sakthi Auto Components Ltd. Tirupur, India for their technical support in carrying out the experiment work.

REFERENCES

- [1] B. Wang, M. He, G.C. Barber, J.D. Schall, C. Tao, Rolling contact fatigue resistance of austempered ductile iron processed at various austempering holding times, *Wear* **398-399**, 41-46 (2018).
- [2] V.K. Arun, K.A. Sandeep, Characterization and Sliding Wear Analysis of Austempered Ductile Iron, *International Journal of Materials Science and Engineering* **4**, 1-12 (2016).
- [3] P.H.S. Cardoso, C.L. Israel, T.R. Strohaecker, Abrasive wear in Austempered Ductile Irons: A comparison with white cast irons, *Wear* **313**, 29-33 (2014).
- [4] K.S. Vinoth, R. Subramanian, S. Dharmalingam, B. Anandavel, Mechanical and tribological characteristics of Stir-Cast Al-Si10Mg and Self-Lubricating Al-Si10Mg/MoS₂ Composites, *Material Technology* **46**, 497-501(2012).

- [5] P. Silawong, A. Panitchagul, S. Inthidech, N. Akkarapattanagoon, U. Kitkamthorn, Improvement of Abrasion Wear Resistance of Ductile Iron by Two-Step Austempering *Advanced Materials Research* **567**, 58-61 (2012).
- [6] G. Gumienny, Carbodic Bainitic and Ausferritic Ductile Cast Iron, *Archives of Metallurgy and Materials* **58** (4), 1053-1058 (2013).
- [7] M. Babazadeh, H. Asiabi, Wear Characteristics of ADIs; A Comprehensive Review on Mechanisms and Effective Parameters, *Journal of Basic and Applied Scientific Research* **3**, 646-656 (2013).
- [8] Y. Sahin, O. Durak, Abrasive wear behaviour of austempered ductile iron, *Materials & Design* **28**, 1844-1850 (2007).
- [9] A. Bedolla-Jacuinde, F.V. Guerra, M. Rainforth, I. Mejiaa, C. Maldonado, Sliding wear behavior of austempered ductile iron microalloyed with boron, *Wear* **330-331**, 23-31 (2015).
- [10] Y. Cheng, P. Jin, J. Liu, G. Li, Effect of boron on the microstructure and mechanical properties of carbidic austempered ductile iron, *Materials Science and Engineering: A* **529**, 321-325 (2011).
- [11] R. Jhala, K. Kothari and S. Khandare, Geometry and size optimization for a steering knuckle with no changes in attachment geometry by reducing production cost and weight, *International Journal of Advanced Engineering & Application* **13**, 1619-1632 (2009).
- [12] S. Madhusudhanan, I. Rajendran, B. Raguganeshkumar, Fatigue Analysis of Steering Knuckle using Finite Element Simulation: Technical Note, *International Journal of Vehicle Structures & Systems* **9** (3), 142-144 (2017).
- [13] A.M. Omran, G.T. Abdel-Jaber and, M.M. Ali, Effect of Cu and Mn on the mechanical properties and microstructure of ductile cast iron, *International Journal of Engineering Research and Application* **4**, 90-96 (2014).
- [14] S. Panneerselvam, K. Putatunda, R. Gundlach, J. Boileau, Influence of intercritical austempering on the microstructure and mechanical properties of austempered ductile cast iron (ADI), *Materials Science and Engineering: A* **694**, 72-80 (2017).
- [15] Y. Yürektürk, M. Baydoğan, Characterization of ferritic ductile iron subjected to successive aluminizing and austempering, *Surface and Coatings Technology* **347**, 15 142-149 (2018).
- [16] J. Kaleicheva, Wear Behavior of Austempered Ductile Iron with Nano sized Additives *Tribology in Industry* **36**, 74-78(2014).
- [17] W. Pachla, A. Mazur, J. Skiba, M. Kulczyk, S. Przybysz, Effect of Hydrostatic Extrusion with Back Pressure on Mechanical Properties of Grey and Nodular Cast Irons, **56** (4), 945-953 (2012).
- [18] N. Selvakumar, T. Ramkumar, Effect of particle size of B₄C reinforcement on Ti-6Al-4V sintered composite prepared by mechanical milling method. *Transactions of the Indian Ceramic Society* **76** (1), 37-37 (2017).
- [19] A. Zammit, S. Abela, L. Wagner, M. Mhaede, M. Grech, Tribological behaviour of shot peened Cu-Ni austempered ductile iron, *Wear* **302**, 829-836 (2013).
- [20] A. Kumar Das, J. Dhal, R. Kumar Panda, S.C. Mishra, S. Sen, Effect of Alloying Elements and Processing Parameters on Mechanical Properties of Austempered Ductile Iron, *Journal of Materials and Metallurgical Engineering* **3**, 8-16 (2013).
- [21] Lei Rao, Wei-Wei Tao, Shuang-Jun Wang, Influence of the composition ratio of manganese and copper on the mechanical properties and the machining performance of ductile iron, *Indian Journal of Engineering and materials Science* **21**, 573-579 (2014).
- [22] N. Bhople, N. Patil, S. Mastud, The Experimental Investigations into Dry Turning of Austempered Ductile Iron, *Procedia Manufacturing* **20**, 227-232 (2018).
- [23] A. Vasko, Chosen factors influencing microstructure and mechanical properties of austempered ductile iron, *Materials Engineering* **16**, 11-14 (2009).
- [24] N. Selvakumar, T. Ramkumar, Effect of high temperature wear behaviour of sintered Ti-6Al-4V reinforced with nano B₄C particles. *Transaction of the Indian Institute of Metals*. **69** (6), 1267-1276 (2016).
- [25] C. Brunetti, L.P. Belotti, M.H. Miyoshi, Influence of Fe On The Room And High-Temperature Sliding Wear Of Nial Coatings, *Surface Coating Technology* **258**, 160-167 (2014).
- [26] A.R. Ghaderi, M. Nili Ahmadabadi, H.M. Ghasemi, Effect of graphite morphologies on the tribological behavior of austempered cast iron, *Wear* **255**, 410-416 (2003).
- [27] T. Ramkumar, P. Narayanasamy, M. Selvakumar, P. Balasundar Effect of B₄C Reinforcement on the Dry Sliding Wear Behaviour of Ti-6Al-4V/B₄C Sintered Composites Using Response Surface Methodology. *Archives of Metallurgy and Materials* **63** (3), 1179-1200 (2018).
- [28] J. Yang, K. Putatunda, Effect of microstructure on abrasion wear behavior of austempered ductile cast iron (ADI) processed by a novel two-step austempering process **406**, 217-228 (2005).